

## Research Article

## Highly Selective Removal of toxic metal ions from Wastewater using Yemeni Limestone as a Natural and Low-Priced Adsorbent: behavior and mechanism

Amer Al Hariri<sup>1</sup>, Yahiya Kadaf Manea<sup>2\*</sup>, Shaif Mohammed Qasem<sup>1\*</sup>,<sup>1</sup>Department of Chemistry, Faculty of Science- University of Aden, Aden, Yemen<sup>2</sup>Department of Chemistry, Faculty of Education - University of Aden, Aden,-Yemen<https://doi.org/10.47372/uajnas.2024.n2.a06>

ARTICLE INFO	Abstract
Received: 10/11/ 2024 Accepted: 12/12/ 2024	The current study examines the use of rock debris leading from mining in the Nakleen zone. The values of these rock wastes must be considered in a feasibility analysis, especially in light of potential ongoing mining operations. Treated Limestone obtained from different areas of Yemen was applied to adsorb Cd (II) and Pb (II) from wastewater. Treated limestone samples were characterized using various techniques, via FTIR, XRF, and TGA-DTA. Batch experiments were conducted with varying pH (2–9), Metal ions concentration (10–50 mg/L), stirring time (10–60 min), and limestone dosage (0.1–1.1 g/50 mL). The ICP-OES analysis was applied to determine the removal percentage of the Cd(II) and Pb(II) ions using the adsorption process. Results show that the limestone was efficient for removing Pb (II) and Cd (II) ions with efficiencies of 99 %, and 98.5 %, respectively. The adsorption of Cd(II) and Pb(II) ions onto limestone obeyed the Freundlich model due to electrostatic affinity. The maximum adsorption capacities of Nak-Cd <sup>+2</sup> and Nak-Pb <sup>+2</sup> after a short time are 6.09 and 4.769 mg/g, respectively. This result indicates that the intercalation of several ions with Nak limestone was better suited to Cd <sup>+2</sup> ions. The enhancement is attributed to the selectivity of adsorption sites in the Nak sample to Cd <sup>+2</sup> ions
<b>Keywords:</b> <i>Yemeni Limestone,</i> <i>Toxic metals,</i> <i>Adsorption</i>	

## 1. Introduction

The hazardous substances and toxic heavy metals such as Lead Pb(II) and cadmium Cd(II) are nowadays environmental priority pollutants due to their characteristics of toxicity, and biological accumulation, which could destroy the ecosystem[1–3]. Therefore, various methods, such as membrane cells, ion exchange, electrochemical participation, adsorption, etc., have been widely used to eliminate metal ions from aquatic environments[4,5]. Ion exchange or adsorption using absorbents has been identified as more effective than other techniques for treating natural water contaminated by heavy metals[6,7][8]. This is due to its benefits, which include its adaptability and simplicity in design, ease of use, rapidness, efficacy, appropriateness, and eco-friendliness characteristics [9,10]. Nevertheless, extracting heavy metals from natural water using universal cation ion exchangers or adsorbents (such as activated carbon, zeolite, and montmorillonite) can be prohibitively

expensive due to their substantial requirements. As a result, there has been a growing interest in recent years in developing cost-effective and environmentally friendly adsorbents through the synthesis of materials using inexpensive raw resources. Mineral materials have emerged as the "Green Materials" of the 21st century. Numerous low-cost and abundant minerals have been widely employed as adsorbents or as raw materials in the creation of efficient adsorbents aimed at extracting heavy metals from natural water sources. Prior research has demonstrated that pure montmorillonite, containing aluminum and magnesium in the octahedral sheet, can be synthesized within the MgO–Al<sub>2</sub>O<sub>3</sub>–SiO<sub>2</sub> systems under autogenous pressure. Reyes and Fiallo reported the successful transformation of illite into a highly crystalline faujasite-type zeolite through fusion with NaOH pellets at 600 °C, followed by hydrothermal treatment. Additionally, clay minerals such as montmorillonite and zeolite exhibit the ability to adsorb heavy metals through cation exchange and the formation of inner-sphere

\* Correspondence to: University of Aden- Yemen

E-mail address: [yahiaka.chem.edu@aden-univ.net](mailto:yahiaka.chem.edu@aden-univ.net) <https://orcid.org/0000-0002-0029-3646>

complexes involving Si–O and Al–O groups[11,12]. Gehlenite et. al has been synthesized via a solid-state reaction of mechanochemically treated mixtures of kaolinite, calcite, and aluminum hydroxide at 900 °C, demonstrating a high capacity for metal ion absorption.[13] To synthesize these three effective adsorbents through calcination in the CaO–MgO–SiO<sub>2</sub>–Al<sub>2</sub>O<sub>3</sub> system[14]. This study selected low-cost and abundant mineral materials, including Yemeni Limestone (Nak, AB1, AB2), as sources of silicon and aluminum. Limestones are sedimentary rocks composed principally of calcium carbonate (calcite) or the double carbonate of calcium and magnesium (dolomite)[15,16]. It is commonly employed in several applications due to its inexpensive cost and widespread availability in nature. Limestones are a well-liked adsorbent for different types of pollutants i.e. organic pollutants, toxic metals, antibiotics, and hormones owing to their secondary binding site, diverse surface, buffering ability, and repurposing qualities, which are also highly helpful. Limestone may therefore be used as an inexpensive adsorbent in water treatment. Additionally, limestone in microsize exhibits exceptional properties, which have proven to possess high absorption capacity for metal ions, which could produced through a high surface reaction involving mechano-chemically treated of calcite, and dolomite components at 300 °C. To discover the activity and capacity of the aforementioned three effective adsorbents through calcination the surface analysis of AB1–AB2–Nak systems was investigated. This research aims to study the possibility of using limestone rocks to remove heavy ions from contaminated aqueous solutions produced by various industries [17,18]. The limestone is produced in large amounts as byproducts during the manufacturing of stones; Therefore, this study opted for low-cost and abundant natural materials like Limestone and/or dolomite were incorporated to provide smaller radius cations such as Ca (II) and Mg(II), aiming to displace Cd(II) and Pb(II) in the presence competitive ions i.e. Zn(II) and Cu(II) upon the crystal structure of limestone.

## 2. Materials and methods:

### 2.1. Materials

All the reagents utilized in this paper were purchased from BDH Chemicals Ltd, Poole, England. The analytical-grade reagents included zinc nitrate (Zn(NO<sub>3</sub>)<sub>2</sub>·6H<sub>2</sub>O), cadmium nitrate (Cd(NO<sub>3</sub>)<sub>2</sub>), copper nitrate (Cu(NO<sub>3</sub>)<sub>2</sub>), Nitric acid (HNO<sub>3</sub>), sodium hydroxide (NaOH), and lead nitrate (Pb(NO<sub>3</sub>)<sub>2</sub>). A range of metal nitrate solutions was prepared by employing different masses of metal salt during the experimental procedures.

### 2.2. Instrumentation

The chemical composition of the samples was determined by an X-ray fluorescence (XRF) spectrometer (Axios Pw4400, PANalytical, Netherlands). The simultaneous Thermo gravimetry (TG) and Differential thermal analysis (DTA) in the temperature range from 25 °C to 1000 °C were conducted on STA449C, Netzsch, Germany. Its heating atmosphere was air and the heating rate was 10 °C min<sup>-1</sup>. The pH value of LCSM was measured using pH–meter 112 Instrument, Romania, and Orbital Shaker Co. United Kingdom. Fourier transform infrared (FTIR) spectra were recorded using a Perkin-Elmer 1750X spectrophotometer. The mixture was centrifuged and the filtrates were analyzed for the Cd<sup>2+</sup>, Pb<sup>2+</sup>, Zn<sup>2+</sup>, and Cu<sup>2+</sup> levels by ICP-OES instrument, Optima 7300 DV series (PerkinElmer Inc.Tokyo, Japan).

### 2.3. Yemeni Limestone Preparation

The sample of limestone (Nakhleen) was derived from the Lahej Province of Yemen. The second and third samples of AB1 and AB2 of Limestone were collected from the quarry zone in Abyan Province, Yemen. The samples were crushed properly, then ground homogeneously to a powder using a mortar and pestle into approximately 3–5 mm diameter grains. The limestone samples underwent cleaning procedures, and the chunks of limestone had very irregular forms, so a Soxhlet extraction system was employed. Next, a Soxhlet setup was filled with the crushed grains. As extraction solvents, methanol, and toluene were utilized to produce a colorless toluene eluent, at which point the procedure was completed. The limestone samples were dried in an oven at 80 °C. Then, the dry samples were ground by mortar and pestle into powders. The sizes of the powder particles were controlled by sieving the powder by two meshes, with mesh sizes of 0.3 and 0.5 μm. The sieved particles were collected into a glass sample bottle and sealed for later use. Analytical grade compounds were all that were employed in this investigation.

### 2.4. Adsorption processes

To carry out the adsorption tests, 1g of limestone sample (AB1, AB2, and NAK) was transferred into 100 mL of the volumetric flask using the proper sieve size as natural adsorbents. Thirty milliliters of a 20 ppm metal ion solution were then added. For 120 minutes, the mixture was agitated at a steady 800 rpm with sporadic shaking. The liquid supernatant was then filtered using 0.454 μm filtering paper. The ultimate equilibrium concentration of Cd<sup>2+</sup> and Pb<sup>2+</sup> ions was determined using the ICP-AES technique. The metal ions were mixed with certain quantities of AB1, AB2, and Nak by adjusting the optimum conditions. The removal percentage (R %) and the amount of metal ions adsorbed (qe) were calculated using the following equations:

$$R\% = \left( \frac{C_o - C_e}{C_e} \right) \times 100 \dots \dots \dots (1)$$

$$q_e(mg/g) = \frac{R\%}{100} \times \left( \frac{V}{m} \right) * C_o \dots \dots \dots (2)$$

Where  $C_i$  and  $C_e$  explain the initial and equilibrium concentrations of heavy metals ( $Pb^{2+}$ , and  $Cd^{2+}$ ), respectively, and  $q_e$  is the amount adsorbed. The adsorbent weight is denoted by  $m$ , while the solution volume is represented by  $V$ . To achieve optimum adsorption of  $Cd^{2+}$  and  $Pb^{2+}$  ions, the experiment was conducted under different parameters such as the effect of solution pH, contact time, initial metal concentration, amount of adsorbent, and temperature using the ICP-AES instrument.

### 3. Results and Discussions

#### 3.1. Adsorption process

This study aimed to exploit limestone as an eco-friendly-adsorbent to eliminate heavy metal ions from wastewater. Although adsorption is a highly promising and efficient method, it suffers from the use of relatively expensive materials as adsorbents.

#### 3.2. Characterization of Yemeni Limestone (Y-LME)

The main chemical composition of Y-LME determined using XRF, for the NAK sample was 49.9.9 % CaO, 3.4 %  $SiO_2$ , 0.3499 %  $SO_3$ , 1.14%  $Al_2O_3$ , 0.183 %  $Fe_2O_3$ , 5277% MgO, 0.3042%  $K_2O$ . The high contents of  $SiO_2$ ,  $Al_2O_3$ , and CaO would contribute to the high removal of metals due to the presence of silanol sites ( $\equiv Si-OH$ ) and aluminols ( $\equiv Al-OH$ ) groups at the surface of Y-LME. The FTIR analysis was employed to investigate the main absorption bands of limestones. Figure 1 shows the Y-LME spectra in the 400-4000  $cm^{-1}$  wavenumber that explains the vibrations of the crystallographic axes for the carbon and oxygen atoms. The strongest bands at 1393 - 1404  $cm^{-1}$ , 870  $cm^{-1}$ , and 710  $cm^{-1}$  corresponded to the basic vibrations of the  $CO_3^{2-}$  ion. Broadening of the band around 1404  $cm^{-1}$  indicates the existence of one or more crystalline forms in the sample.

When one mineral predominates, broadening decreases, and a "shoulder" emerges on either the shorter or longer wavelength side, adjacent to the dominant form's peak [19]. The shape of this band indicates that the sample is composed of a distinct crystalline structure.

The band at 874  $cm^{-1}$ , which corresponds to the single frequency  $\nu_2$ , is caused by an out-of-plane bend in the C-O bond. The fundamental frequency  $\nu_4$  at 710  $cm^{-1}$  in the spectrum is attributed to the planar bending vibration.

This band makes it possible to distinguish the different crystalline phases of limestone. Indeed, the investigations showed that it appears at 710  $cm^{-1}$  in calcite, at 744  $cm^{-1}$  in vaterite, and as a doublet at 700  $cm^{-1}$  and 713  $cm^{-1}$  in aragonite [20].

This result shows that the limestones used in this study are a calcite crystalline phase. The two low-intensity bands around 1797  $cm^{-1}$  and 2512  $cm^{-1}$  are respectively assigned to the combinations of the frequencies  $\nu_1 + \nu_4$  and  $\nu_1 + \nu_3$  [21]. These bands allow us to find the frequency of the fundamental vibration  $\nu_1$  inactive in IR at 1085  $cm^{-1}$ . This value is consistent with the result (1088  $cm^{-1}$ ) derived from the polarized Raman spectra of calcite by Porto et al. [22]. This outcome further demonstrates that the sample is entirely composed of calcite. According to the literature, the bands at around 3100  $cm^{-1}$  and 3457  $cm^{-1}$  are attributed to the symmetric and anti-symmetric stretching of the water's O-H bond, respectively. [23][24].

Fig.2a shows a tiny peak at 200°C belongs to the loss of ore's moisture content while the second very sharp small narrow peak may result from the loss of crystallization water content. The calcination of the lime-stone mineral calcite is the cause of the last broad, wide major endothermic peak. This peak, which begins at 550°C and finishes at around 650°C, represents the breakdown of Y-LSM-Nak (Figure 2c) into carbon dioxide ( $CO_2$ ) and calcium oxide (CaO). Figure 2c's data indicates that the weight remained constant at 56.06 percent. It is assumed that the sample is made up entirely of  $CaCO_3$  based on the mass loss related to  $CaCO_3$  breakdown.

Table 1. Relevant composition chemical composition of the limestone samples

Sample	CaO	$SiO_2$	$Al_2O_3$	$Fe_2O_3$	$K_2O$	MgO	$SO_3$
Nak	49.995	3.411	1.104	0.527	0.304	0.183	0.345
AB.1	47.10	9.04	2.88	1.04	0.28	-	0.21
AB.2	50.25	5.05	1.68	0.50	0.16	-	0.25

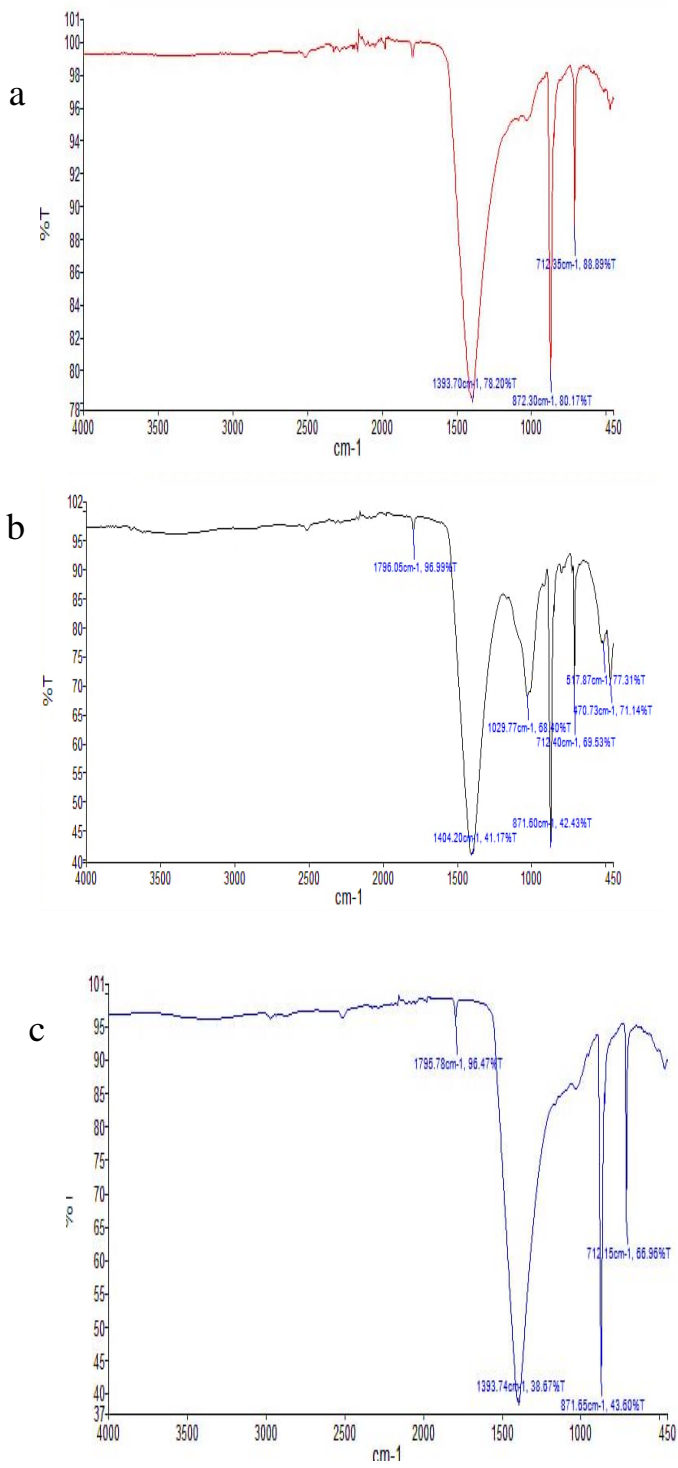


Figure 1: Infrared absorption spectrum of limestone samples AB1 (a), AB2(b), and Nak (c) in the range from 4000 to 400 cm<sup>-1</sup>

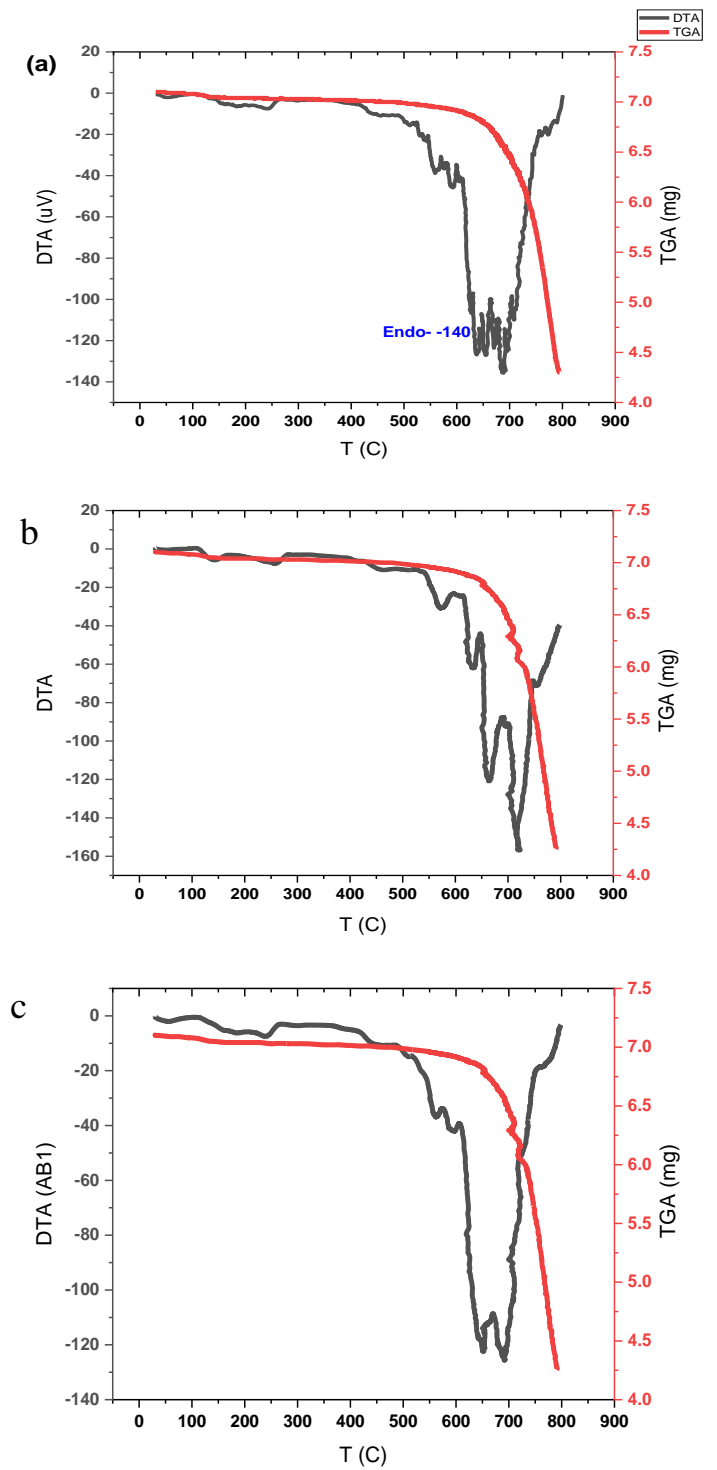


Figure 2: (2): TG-DTA curve in the thermal activation process of LS AB1 (a), AB2 (b), and Nak (c).

### 3.3. Batch Adsorption

In this work, we have selected the Nakleen sample as a natural adsorbent and will expand the work to involve all samples in the next work due to the limited paper size.

### 3.4. Optimum conditions of heavy metals (Pb<sup>2+</sup> and Cd<sup>2+</sup>) removal

#### 3.4.1. Influence of adsorbent dosage

The effect of limestone dosage was studied at different amounts of limestone samples i.e. 0.3, 0.5, 0.8, and 1.1 g as shown in Figure 3a. Adsorption results for Pb<sup>2+</sup> Cd<sup>2+</sup> ions with Nakhleen limestone sample indicate tend to capture Pb<sup>2+</sup> cations. The removal percentage significantly increased from 90.04 and 91.59 %, when 0.3 g of limestone was used, to 96.12 and 98.21 % when 1.1 g of limestone was used to remove the Pb(II) and Cd(II) ions respectively.

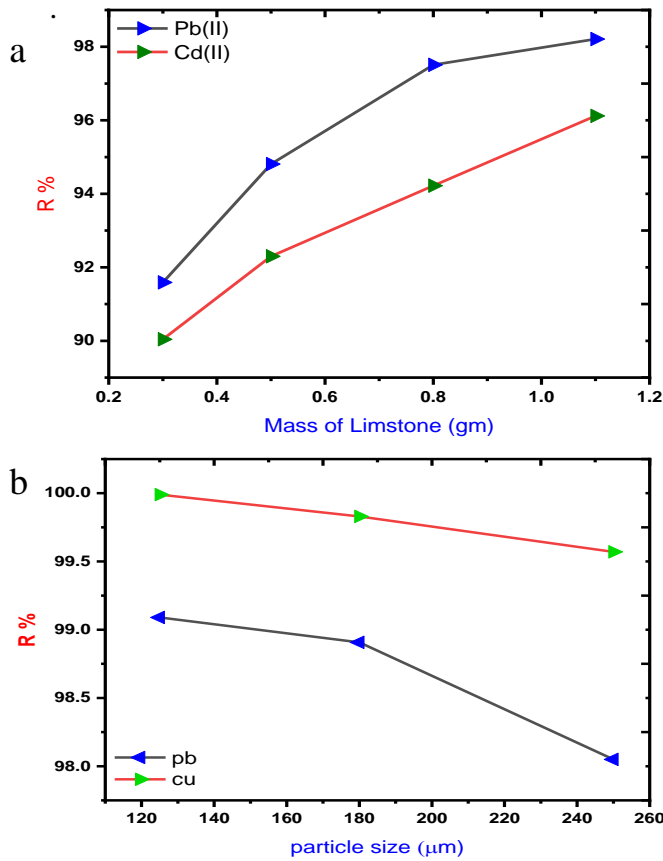


Figure 3: (a) Effect of the mass of limestone on removal percentage of Pb (II) and Cd(II) ions, (b) The relationship between solution pH and removal percentage

The removal percentage of Pb<sup>2+</sup> and Cd<sup>2+</sup> may rise when adsorbent doses of limestone increase. This might be because greater adsorbent dosages increase the sorbent's surface area and pore volume, which increases its adsorption capacity

#### 3.4.2. Effect of particle size

The effect of limestone particle size was studied, where three different particle sizes (125, 180, and 250 μm) were used. The percentage of adsorption was at the maximum when using limestone with a particle size of 125 μm, and it slightly decreased when the particle size increased to 250 μm. As shown in Figure 3b, the lowest percentage of adsorption was obtained using limestone with a particle size of 300 μm. This finding agrees with the fact that increasing the particle size decreases the surface area of contact between the adsorbent and the Pb (II) ion solution.

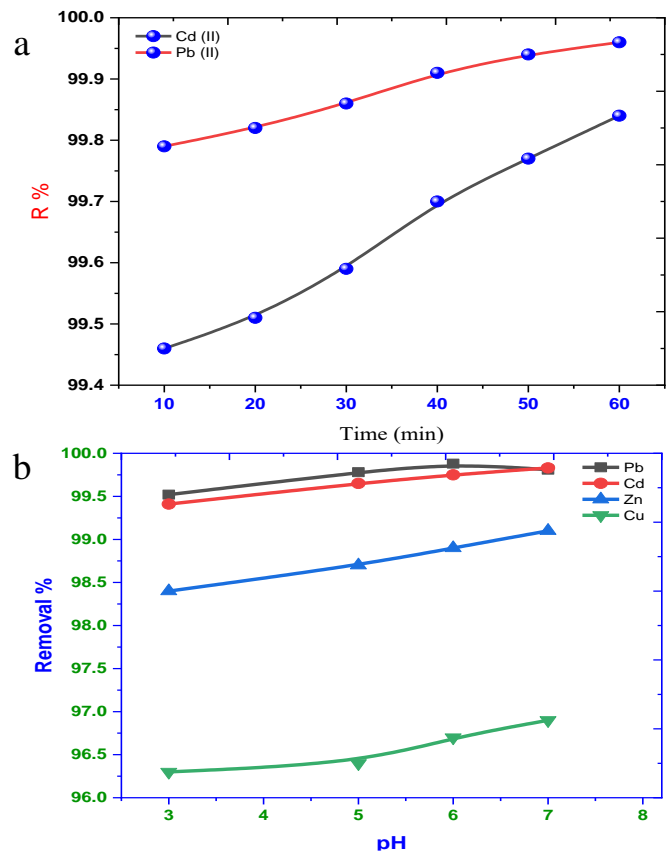


Figure 4: (a) effect of pH value on the adsorption capacity of the Nak-Limestone sample ; (b) Effect of contact time on adsorption efficiency.

Table (2): Adsorption results for Pb<sup>2+</sup>,Cu<sup>2+</sup>,Cd<sup>2+</sup>,andZn<sup>2+</sup> cations with Nakhleen limestone sample

Metal Ion	C <sub>0</sub>	C <sub>f</sub>	Mass of sample	Q <sub>e</sub> μg/g	% R
Cd(II)	20 ppm	0.041 ppm	1.1g	8326	99.79
Pb(II)	20 ppm	0.028 ppm	1.1g.	9328	99.86
Zn(II)	20 ppm	0.21 ppm	1.1g	3297	98.91
Cu(II)	20ppm	0.85 ppm	1.1g	3191	95.75

### 3.4.3. Influence of solution pH

The pH is considered one of the factors affecting the adsorption process, as hydrogen ions compete with the studied metal ions for adsorption sites. Also, hydroxide ions can precipitate metal ions if their concentration is high in the solution. To find the effect of the initial solution pH on the adsorption capacity of  $Pb^{+2}$  and  $Cd^{+2}$  ions by Nak limestone, the effect of pH was studied at the pH range of 3–7.

The relationship between the adsorption rate and pH is shown in Figure 4a. High effective competition between cations ( $Pb(II)$  and  $H^+$ ) for the same vacant sites was the reason for the low uptake at strongly acidic conditions (pH  $\approx$  3). However, mildly acidic (pH = 4–6) led to less effective competition, therefore adsorption increased when pH was raised further. The maximum adsorption capacities for  $Pb^{+2}$  ions were achieved at pH = 6. The limestone adsorption rate was 99.88%.

### 3.3.4. Effect of contact time

The effect of contact time was investigated for the experimental data to comprehend the uptake processes of metal ions using the Nak-limestone samples, as illustrated in Figure 4b.

### 3.3.5. Co-removal of $Pb^{+2}$ and $Cd^{+2}$ ions

The adsorption capacity of Yemeni limestone adsorbents (NaK) may be impacted by competitive behavior since heavy metals often coexist in polluted wastewater systems. Competitive adsorption experiments of the ternary system were conducted to assess the impact of coexisting Pb, and Cd on the adsorption capacity of limestone.

### 3.3.5. Adsorption isotherms

To describe time-dependent adsorption of  $Pb^{+2}$  and  $Cd^{+2}$  by Nak-limestone adsorbent, isotherm adsorption was conducted by mixing 50 mL of metal ions (20 ppm) solution with 1.1 g of adsorbent in the range of time 5–120 min (Figure 5a,b,c). To investigate the metal ions uptake on the Nak-limestone surface, we have drawn the relationship between the maximum amounts adsorbed ( $Q_m$ ) and the amount adsorbed at equilibrium as shown in Figure 5a

As shown in Figure 5a, the maximum adsorption capacities of Nak- $Cd^{+2}$  and Nak- $Pb^{+2}$  after 30 min are 6.09 and 4.769 mg/g, respectively. This result indicates that the intercalation of several ions with Nak limestone was better suited to  $Cd^{+2}$  ions. The enhancement is attributed to the selectivity of adsorption sites in the Nak sample to  $Cd^{+2}$  ions. The two models' fitted graphs and correlation parameters are presented in Figure 5(b and c).

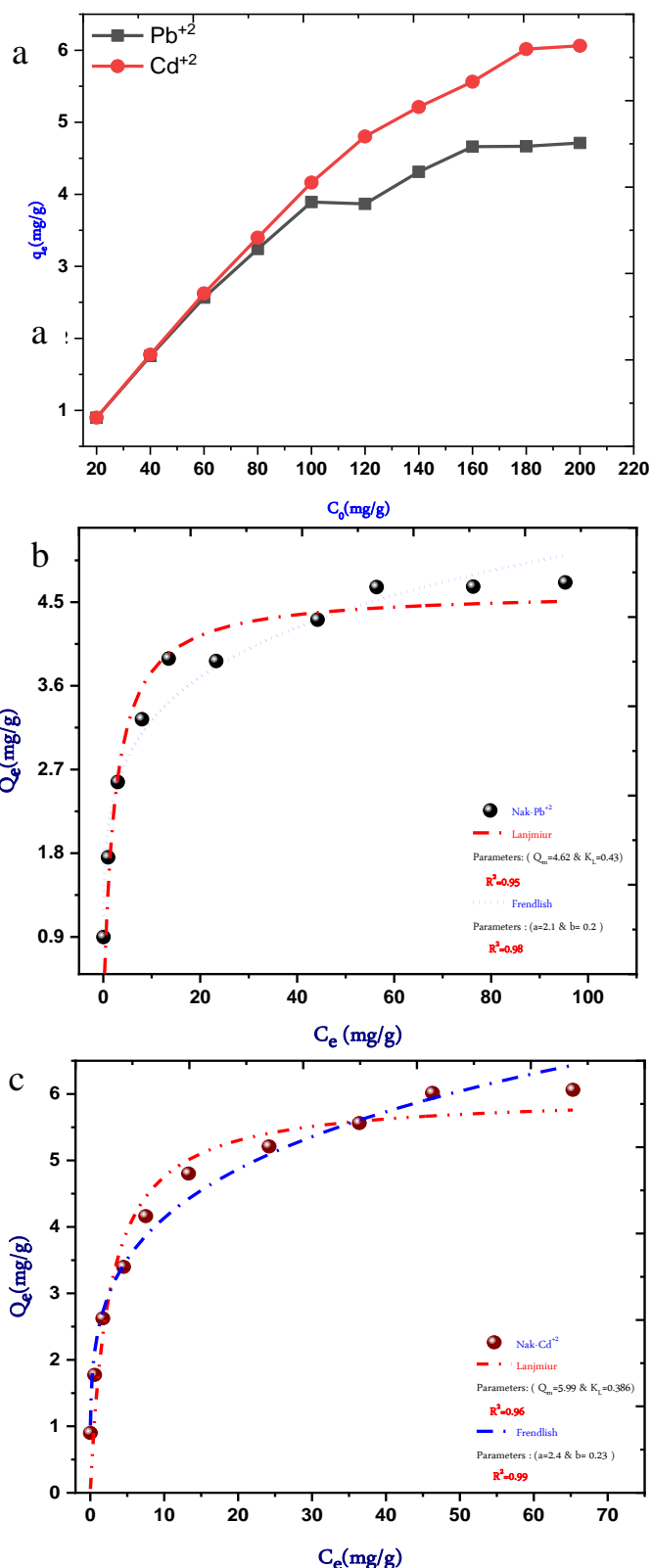


Figure 5: comparison analysis for metal ions uptake on the surface of Nak-limestone (a); Simulated adsorption isotherm and the corresponding trending lines obtained by fitting the data by Langmuir and Freundlich equations for the removal  $Pb^{+2}$  (b) and  $Cd^{+2}$  (c).

According to the correlation coefficient ( $R^2$ ), the Freundlich model showed the highest ( $R^2$ ) values for both Cd(II) and Pb(II) on Nak limestone adsorbents. Consequently, the results suited the Freundlich model better than the Langmuir model. It indicates that the active sites on the surface of Nak are homogeneous and adsorb  $Pb^{+2}$  and  $Cd^{+2}$  ions in a multilayer adsorption manner. It can be surmised that the conventional Nak-Limestone captures  $Pb^{2+}$  and  $Cd^{2+}$  ions mainly through the interlayer  $COO^-$  anion, which is accompanied by precipitation and chelation reactions and exhibits multilayer adsorption. At this point it is important to provide some comments about the use of linear forms of the Langmuir isotherm as shown in Fig 6 a,b. It can describe different forms of Langmuir model using variable  $q_e$  for the definition of both independent and dependent variables, which may lead to inconsistent definition of measurement fluctuations.

### 3.4.4. Wastewater treatment

Lime allows water to be softened, purified, have its cloudiness eliminated, its acidity to be neutralized and its impurities to be eliminated.

Table (3): Adsorption processes for wastewater sample by Nak-Limestone

cation	Wastewater before adsorption by Lamiston	Wastewater after adsorption by Lamiston
$Pb^{+2}$	0.466ppm	0.207ppm

### Conclusion

The adsorption efficiency of yemeni limestone was investigated. The ICP-OES analysis was applied to determine the removal percentage of the Cd(II) and Pb(II) ions using the adsorption process. Results show that the limestone was efficient for removing Pb (II) and Cd (II) ions with efficiencies of 99 %, and 98.5 % respectively. The adsorption of Cd(II) and Pb(II) ions onto limestone obeyed the Freundlich model due to electrostatic affinity.

### Acknowledgments

The authors gratefully acknowledge the Department of Chemistry, University of Aden for providing instrumental facility.

### Disclosure

The authors should clear the conflicts of interest in their work.

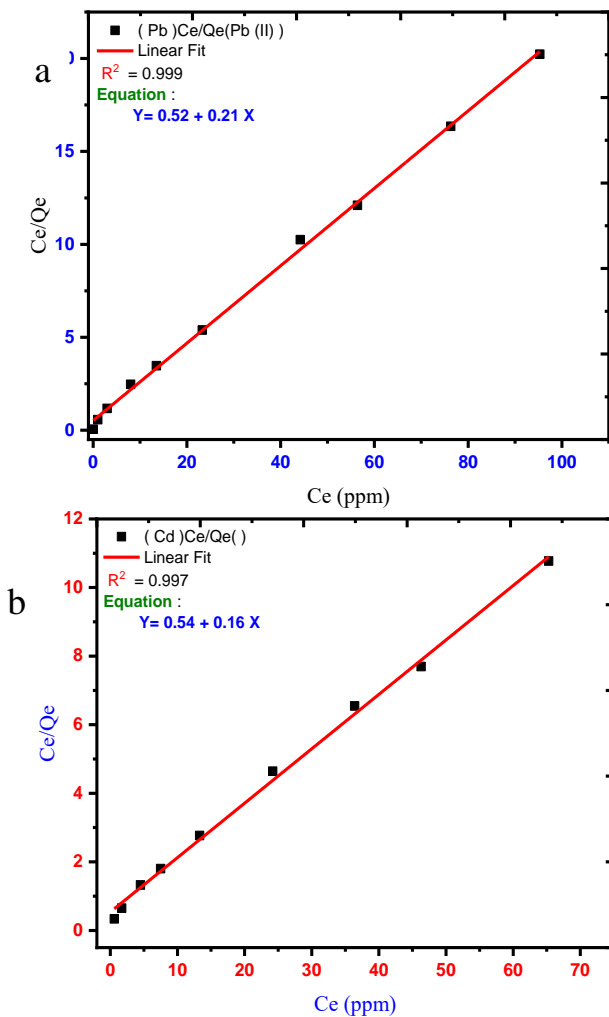


Fig6: Langmuir isotherm for Pb(II) removal and (b) for Cd(II) with various initial solution concentrations using Nak limestone (c).

## 4. References

- [1] F.A.M. Alahdal, M.T.A. Qashqoosh, Y.K. Manea, R.K.A. Mohammed, S. Naqvi, Green synthesis and characterization of copper nanoparticles using Phragmanthera austroarabica extract and their biological/environmental applications, *Sustain. Mater. Technol.* 35 (2023). <https://doi.org/10.1016/j.susmat.2022.e00540>.
- [2] A.M. Omer, G.S. Elgarhy, G.M. El-Subruiti, E.M. Abd El-Monaem, A.S. Eltaweil, Construction of efficient Ni-FeLDH@MWCNT@Cellulose acetate floatable microbeads for Cr(VI) removal: Performance and mechanism, *Carbohydr. Polym.* 311 (2023). <https://doi.org/10.1016/j.carbpol.2023.120771>.
- [3] A.A. Wani, A.M. Khan, Y.K. Manea, M.A.S. Salem, M. Shahadat, Selective adsorption and ultrafast fluorescent detection of Cr(VI) in wastewater using neodymium doped polyaniline supported layered double hydroxide nanocomposite, *J. Hazard. Mater.* 416 (2021) 125754. <https://doi.org/10.1016/J.JHAZMAT.2021.125754>.
- [4] N.S. Razali, A.S. Abdulhameed, A.H. Jawad, Z.A. AlOthman, T.A. Yousef, O.K. Al-Duaij, N.S. Alsaiani, High-Surface-Area Activated Carbon Derived from Mango Peels and Seeds Wastes via Microwave-Induced ZnCl<sub>2</sub> Activation for Adsorption of Methylene Blue Dye Molecules: Statistical Optimization and Mechanism, *Molecules* 27 (2022). <https://doi.org/10.3390/MOLECULES27206947>.
- [5] S.A. Razzak, M.O. Faruque, Z. Alsheikh, L. Alsheikhmohamad, D. Alkuroud, A. Alfayez, S.M.Z. Hossain, M.M. Hossain, A comprehensive review on conventional and biological-driven heavy metals removal from industrial wastewater, *Environ. Adv.* 7 (2022) 100168. <https://doi.org/10.1016/J.ENVADV.2022.100168>.
- [6] Y. Zhang, Q. Ma, M. Chen, Y. Wang, J. Tian, X. Wang, X. Wang, Z. Chen, X. Wang, Effects of different covalent organic frameworks structures on radioactive iodine adsorption, *J. Environ. Chem. Eng.* 12 (2024). <https://doi.org/10.1016/j.jece.2024.114193>.
- [7] X. Zheng, O. Alam, Y. Zhou, D. Du, G. Li, W. Zhu, Heavy metals detection and removal from contaminated water: A critical review of adsorption methods, *J. Environ. Chem. Eng.* 12 (2024) 114366. <https://doi.org/10.1016/J.JECE.2024.114366>.
- [8] A. Mumtaz, Y. Kadaf, S. Ashfaq, Synthesis and Characterization of Nanocomposite Acrylamide TIN (IV) Silicomolybdate: Photocatalytic Activity and Chromatographic Column Separations 1, 74 (2019) 330–338. <https://doi.org/10.1134/S1061934819040026>.
- [9] Y.K. Manea, A.M. Khan, A.A. Wani, M.A.S. Saleh, M.T.A. Qashqoosh, M. Shahadat, M. Rezakazemi, In-grown flower like Al-Li/Th-LDH@CNT nanocomposite for enhanced photocatalytic degradation of MG dye and selective adsorption of Cr(VI), *J. Environ. Chem. Eng.* (2021) 106848. <https://doi.org/10.1016/J.JECE.2021.106848>.
- [10] M.A.S. Salem, A.M. Khan, Y.K. Manea, A.A. Wani, Nano chromium embedded in f-CNT supported CoBi-LDH nanocomposites for selective adsorption of Pb<sup>2+</sup> and hazardous organic dyes, *Chemosphere* 289 (2022) 133073. <https://doi.org/10.1016/J.CHEMOSPHERE.2021.133073>.
- [11] M. Shahadat, A.A. Wani, Y.K. Manea, R. Adnan, S.Z. Ahammad, S.W. Ali, Heavy metals scavenging using multidentate/multifunctional aerogels and their composites, *Adv. Aerogel Compos. Environ. Remediat.* (2021) 275–296. <https://doi.org/10.1016/B978-0-12-820732-1.00015-1>.
- [12] Y.K. Manea, A.M. Khan, Enhanced photocatalytic degradation of methylene blue and adsorption of metal ions by SDS-TiP nanocomposite, *SN Appl. Sci.* 1 (2019). <https://doi.org/10.1007/s42452-019-0817-5>.
- [13] K. Weise, N. Ukrainczyk, E. Koenders, Pozzolanic Reactions of Metakaolin with Calcium Hydroxide: Review on Hydrate Phase Formations and Effect of Alkali Hydroxides, Carbonates and Sulfates, *Mater. Des.* 231 (2023) 112062. <https://doi.org/10.1016/J.MATDES.2023.112062>.
- [14] V.K. Jha, Y. Kameshima, K. Okada, K.J.D. Mackenzie, Ni<sup>2+</sup> uptake by amorphous and crystalline Ca<sub>2</sub>Al<sub>2</sub>SiO<sub>7</sub> synthesized by solid-state reaction of kaolinite, *Sep. Purif. Technol.* 40 (2004) 209–215. <https://doi.org/10.1016/J.SEPPUR.2004.02.010>.
- [15] D.F. Valezi, B.L.S. Vicentin, A.C.G. Mantovani, E. Di Mauro, Applications of electron magnetic resonance in the study of soils, minerals, and iron oxides, *Exp. Methods Phys. Sci.* 50 (2019) 203–217. <https://doi.org/10.1016/B978-0-12-814024-6.00010-8>.
- [16] F.L. Schwab, *Sedimentary Petrology*, *Encycl. Phys. Sci. Technol.* (2003) 495–529. <https://doi.org/10.1016/B0-12-227410-5/00678-5>.
- [17] Y. Kadaf Manea, A. Banu, M.T.A. Qashqoosh, A. Mumtaz Khan, F.M.A. Alahdal, A. Ahmad Wani, M.A.S. Salem, S. Naqvi, Interaction of AMOT@CS NPs and AMOT drug with bovine serum albumin: Insights from spectroscopic and molecular docking techniques, *Chem. Phys.* 546 (2021) 111139. <https://doi.org/10.1016/J.CHEMPHYS.2021.111139>.
- [18] A.A. Wani, A.M. Khan, Y.K. Manea, M. Shahadat, S.Z. Ahammad, S.W. Ali, Graphene-supported organic-inorganic layered double hydroxides and their environmental applications: A review, *J. Clean. Prod.* 273 (2020) 122980. <https://doi.org/10.1016/J.JCLEPRO.2020.122980>.
- [19] Y.K. Manea, A.M. Khan, S.A. Nabi, Facile synthesis of Mesoporous Sm@POA/TP and POA/TP nanocomposites with excellent performance for the photocatalytic degradation of MB and MG dyes, *J. Alloys Compd.* 791 (2019) 1046–1062. <https://doi.org/10.1016/J.JALLCOM.2019.03.091>.
- [20] S. Nabi, M. Shahadat, R. Bushra, ... A.S.-C.E., undefined 2010, Development of composite ion-exchange adsorbent for pollutants removal from environmental wastes, Elsevier (n.d.). <https://www.sciencedirect.com/science/article/pii/S1385894710007928> (accessed April 14, 2020).
- [21] Y.K. Manea, A.M.T. Khan, M.T.A. Qashqoosh, A.A. Wani, M. Shahadat, Ciprofloxacin-supported chitosan/polyphosphate nanocomposite to bind bovine serum albumin: Its application in drug delivery, *J. Mol. Liq.* 292 (2019) 111337. <https://doi.org/10.1016/j.molliq.2019.111337>.
- [22] H. Kitagawa, T. Mitani, Valence transition with charge ordering in a conductive MMX-chain complex, *Coord. Chem. Rev.* 190–192 (1999) 1169–1184. [https://doi.org/10.1016/S0010-8545\(99\)00174-5](https://doi.org/10.1016/S0010-8545(99)00174-5).
- [23] A. Banu, R.H. Khan, M.T.A. Qashqoosh, Y.K. Manea, M. Furkan, S. Naqvi, Multispectroscopic and computational studies of interaction of bovine serum albumin, human serum albumin and bovine hemoglobin with bisacodyl, *J. Mol. Struct.* 1249 (2022) 131550. <https://doi.org/10.1016/J.MOLSTRUC.2021.131550>.
- [24] M.T.A. Qashqoosh, F.A.M. Alahdal, Y.K. Manea, S.M. Zakariya, S. Naqvi, Synthesis, characterization and spectroscopic studies of surfactant loaded antiulcer drug into Chitosan nanoparticles for interaction with bovine serum albumin, *Chem. Phys.* 527 (2019). <https://doi.org/10.1016/j.chemphys.2019.110462>.
- [25] N.M. Ahmed, S.K. Saleh, O.A. Mansha, Estimation of limestone deposits calcium carbonate source for industrial applications in some area of Lahej Governorate- Yemen, *Univ. Aden J. Nat. Appl. Sci.* 24 (2020) 423–438. <https://doi.org/10.47372/UJNAS.2020.N2.A10>.
- [26] A.A. Wani, A.M. Khan, Y.K. Manea, M. Singh, Facile synthesis of layered superparamagnetic Fe<sub>3</sub>O<sub>4</sub>-MoS<sub>2</sub> nanosheets on chitosan for efficient removal of chromium and ciprofloxacin from aqueous solutions, *J. Water Process Eng.* 51 (2023) 103340. <https://doi.org/10.1016/J.JWPE.2022.103340>.
- [27] Z. Al-Shadidi, Moisture and temperature effects on rocks materials and natural erosion energy, *Univ. Aden J. Nat. Appl. Sci.* 21 (2017) 413–420. <https://doi.org/10.47372/UJNAS.2017.N2.A20>



## بحث علمي

## الإزالة الانتقائية العالية لأيونات المعادن السامة من المياه العادمة باستخدام الحجر الجيري اليميني كمادة ماصة طبيعية

## ومنخفضة السعر: السلوك والآلية

عامر الحريري<sup>1</sup>، يحيى كداف مانع<sup>2</sup>، شائف محمد قاسم<sup>1</sup>  
قسم الكيمياء - كلية العلوم، جامعة عدن<sup>1</sup>

قسم الكيمياء - كلية التربية - جامعة عدن<sup>2</sup>

<https://doi.org/10.47372/uajnas.2024.n2.a06>

## الملخص

## مفاتيح البحث

التسليم: 2024/11/10

القبول: 2024/12/12

## كلمات مفتاحية:

الامتزاز،  
العناصر الثقيلة،  
الحجر الجيري اليميني

تتناول الدراسة الحالية استخدام حطام الصخور الناتج عن التعدين في منطقة ناكلين - محافظة لحج . يمكن أخذ قيم هذه الفتات الصخرية بعين الاعتبار في تحليل الجدوى، خاصة في ضوء عمليات التعدين المحتملة. في هذه الدراسة تم تطبيق الحجر الجيري المعالج المستخرج من مناطق مختلفة في اليمن لامتصاص أيونات الكاديوم (Cd II) والرصاص (Pb II) من المياه العادمة. كما تم تشخيص عينات الحجر الجيري المعالج باستخدام تقنيات متنوعة، من خلال FTIR و XRF و TGA-DTA. كذلك تم إجراء تجارب الامتزاز مع درجات الحموضة المختلفة والتي تقع ما بين (2-9)، وكان وتركيز أيونات المعادن المدروسة (10-50 ملغ/لتر)، ومدة التجربة ما بين (10-60 دقيقة)، ووقد كانت كميات الحجر الجيري تتراوح ما بين (0.1-1.1 غم/50 مل). لمعرفة كفاءة الحجر الجيري في عملية الامتزاز تم تطبيق تحليل ICP-OES لتحديد نسبة إزالة أيونات Cd(II) و Pb(II). أظهرت النتائج أن الحجر الجيري كان فعالاً في إزالة أيونات Pb(II) و Cd(II) بكفاءة بلغت 99% و 98.5% على التوالي. وأظهرت نتائج ان الامتزاز لأيونات Cd(II) و Pb(II) على الحجر الجيري يتبع نموذج فريدلش مما يدل ان الامتزاز على سطح الحجر الجيري يعزى إلى الألفة الكهروستاتيكية الناشئة على سطح الحجر الجيري.